A Deep Learning Framework for Multi-Class Classification of Breast Cancer Abnormalities

R. Subasini, Devi Vijayan
Department of Electronics and Communication Engineering,
Amrita School of Engineering, Coimbatore,
Amrita Vishwa Vidyapeetham, India
v_devi@cb.amrita.edu

2024 4th International Conference on Artificial Intelligence and Signal Processing (AISP) | 979-8-3503-5065-4/24/$31.00 ©2024 IEEE | DOI: 10.1109/AISP61711.2024.10870714

***Abstract*—Breast cancer, impacting both men and women, though it is notably more prevalent in women, ranks among the most widespread types of cancer worldwide. Early detection of breast cancer significantly improves treatment outcomes and increases the likelihood of successful recovery, underscoring the importance of regular screenings and prompt medical attention upon noticing any changes or abnormalities in breast health. Utilizing a Computer-Aided Diagnosis (CAD) system further enhances early detection capabilities, assisting clinicians in accurate diagnosis and treatment planning. Unlike existing binary methods, the proposed method employs a three-class classification system distinguishing between mass, microcalcification, and normal tissues. Initial preprocessing is followed by patch extraction and augmentation, playing a pivotal role in mitigating overfitting and enabling the model to learn robust features that generalize effectively to new medical images. A deep-learning architecture, with various pre-trained models includes ResNet50, ResNet101, ResNet152, Inception ResNet V2, Inception V3, VGG-16, and VGG-19, is trained on the augmented dataset to classify patches into normal, microcalcification, and mass categories. The proposed model is validated on the combined dataset which demonstrates the model's accuracy in diagnosing breast abnormalities, with Inception ResNet V2 achieving an accuracy of 97.93%, outperforming other pre-trained models. The system achieved an overall sensitivity, specificity, precision, and F1-score approximate 0.9411, 0.9885, 0.9740 and 0.9557, respectively, illustrating the model's robustness and its ability to reliably detect and classify breast abnormalities.**

Keywords—Breast cancer, Computer Aided Diagnosis, Inception ResNet V2, mammogram, mass, microcalcification

I. Introduction

Cancer remains a significant global health challenge, claiming nearly 10 million lives in 2020 alone and accounting for nearly one in six deaths [1]. Timely and accurate detection of abnormalities is important in improving treatment outcomes and enhancing survival rates. The complex and subtle nature of abnormalities, particularly in medical imaging, pose significant challenges for accurate diagnosis. Breast cancer is predominantly a life-threatening disease affecting females, but occurrences in males are relatively rare.

In the United States, breast cancer remains a significant concern, with approximately 268,600 invasive instances and 62,930 instances of non-invasive breast cancer reported in 2019 [2]. Globally, the World Health Organization (WHO) estimates 2.1 million annual cases of breast cancer in women, with a 15% fatality rate [3], underscoring the urgent need for improved detection, treatment strategies and including the efforts to reduce false positives in diagnosis to reduce unnecessary anxiety and interventions [4]. Breast abnormalities include masses, microcalcification, asymmetry, and architectural distortion. The existing work in this field concentrates majorly on any one abnormality or concentrates on finding whether the tissue is normal or abnormal rather than concentrating on multiple abnormalities along with finding what abnormality it is.

Medical imaging often unveils a multitude of concurrent abnormalities in patients, necessitating a comprehensive understanding for effective diagnosis. Denser breast tissue may obscure potential abnormalities, leading to decreased sensitivity in detecting cancerous lesions [5,6], including masses and microcalcifications as shown in Fig. 1, serve as crucial indicators, confirmed through biopsies and histopathological analyses as malignant. A mass, a dense tissue lump on mammograms, can be benign or malignant, with its irregularity often indicating a higher likelihood of malignancy [7]. Microcalcification are tiny white specks indicating calcium deposits on mammograms, often indicative of abnormal cell growth. In 2022, microcalcifications on mammography played a significant role, identifying 30-50% of non- palpable breast cancers [8]. Analyzing the distribution, size, and shape of microcalcifications is essential in breast cancer screening and diagnosis. The proposed work aims in developing a Computer Aided Diagnosis (CAD) system specifically targeting breast tissue classification, distinguishing between masses, microcalcifications, and normal tissue, thereby enhancing diagnostic accuracy and aiding in early detection of abnormalities [9].

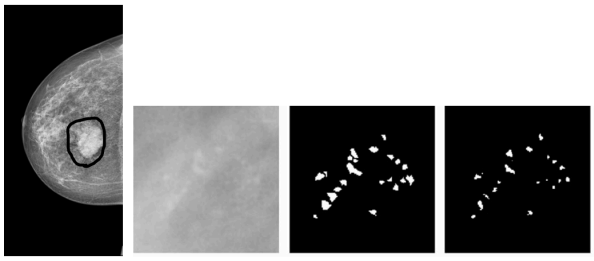

(a) (b)

Fig. 1. (a) Mass (b) Microcalcification

II. Related Work

Majority of the existing research in this domain tends to concentrate solely on identifying a single abnormality or on discerning whether the tissue is malignant or benign. In contrast, our work breaks new ground by focusing on the classification of multiple abnormalities, namely mass, microcalcification, along with normal tissue, offering a more comprehensive diagnostic approach.

Kermouni et al. [10] developed a system focusing on the classification of mammographic regions of interest (ROIs) as

normal or abnormal, specifically targeting microcalcifications. Employing the INbreast dataset, the four-step methodology included mammogram pre-processing, ROI extraction, feature extraction, and classification using k-nearest neighbors (KNN), decision tree, and support vector machine (SVM) classifiers. The SVM classifier demonstrated superior performance, with 98.66% sensitivity, 97.77% specificity, and 98.20% precision.

H. Cao et al. [11] introduced a multi-task U- shaped network for classifying breast masses as malignant or benign. Leveraging transfer learning, label smoothing, and the U-Net short connection mechanism, the system achieved an accuracy of 98.17% on the Digital Database for Screening Mammography (DDSM) dataset and 93.91% on the INbreast dataset. Emphasizing shape and location information, the network architecture provided both classification and segmentation results, addressing challenges including overfitting and weaker generalization.

E. M. F. El Houby et al. [12] proposed a diagnosis system that utilizes deep learning and Convolutional Neural Networks (CNNs) to classify breast mass in mammographic images as malignant or benign. The system emphasizes the challenge of early detection and the difficulty in distinguishing between malignant and benign cases in breast cancer diagnosis. A combination of MIAS, DDSM, INbreast dataset are used as the input to this classification system. The developed system achieves an accuracy of 93.2% on MIAS-INbreast dataset and 90.17 % on MIAS-DDSM-INbreast dataset.

X.Yu et al. [13] presented a diagnostic system for breast abnormality which includes mass and microcalcification classification based on ResNet-50, a deep-learning model. Using a combination of mini-MIAS and INbreast datasets employed the Scaling and Contrast enhancement data augmentation framework (SCDA), the system outperformed other pretrained models. Resnet-34 demonstrated superior classification accuracy, achieving 95.74%.

Cheng-Kai Lu et al. [14] employed a Deep Convolutional Neural Network that allows effective feature extraction from the segmented image, enabling the detection of abnormal masses. The system achieves an accuracy of 95.24% on both MIAS and DDSM datasets.

R. Rabidas et al. [15] employed Local Photometric Attributes (LPA) and evaluating its effectiveness on the mini-MIAS and DDSM datasets. The method incorporated stepwise logistic regression for optimal feature selection and employed Fisher's Linear Discriminant Classifier, achieving the best performance with an accuracy of 86.90% for the mini-MIAS dataset and 80.76% for the DDSM dataset.

A. Baccouche et al. [16] developed a YOLO-based system integrating Cycle GAN and Pix2Pix for classification and simultaneous detection of breast abnormalities on mammograms. The fusion model demonstrated accuracy of 93% and 88% in detecting mass, calcification, and 95% in detecting architectural distortion lesions. Despite promising early detection and classification results, a notable limitation is prolonged training times due to the complexity of hyperparameter optimization in image- to-image techniques.

Shu et al. [17] introduced a mammographic image classification method using deep neural networks, leveraging the INbreast and CBIS-DDSM datasets. Their approach employed deep CNNs to distinguish between malignant and benign mass and microcalcification lesions, introducing region-based pooling structures to enhance performance. Despite reaching a 92% accuracy, the model displayed a tendency to misclassify benign cases as malignant, suggesting areas for improvement.

F.Mohanty et al. [18] presented a CAD model for mammogram classification by utilizing hybridized features extraction through 2D-BDWT, GLCM, PCA, and FOA, achieving 100% accuracy on MIAS and DDSM datasets. These advanced feature extraction techniques enhance the model's ability to discern subtle malignancy patterns. It considers mass, microcalcification, asymmetry, and architectural distortion to identify normal/abnormal mammograms and distinguish benign/malignant cases.

III. Materials and Methods

The proposed work utilizes datasets from INbreast and mini-MIAS, employing preprocessing, patch extraction, data augmentation, and transfer learning techniques to improve diagnostic accuracy.

A. Data Set

The work combines images from mini- MIAS and INbreast datasets for model building. The INbreast dataset includes 115 cases (410 images), featuring various abnormalities which includes masses, microcalcifications, asymmetries, and distortions [19]. The mini-MIAS dataset, consisting of 322 mammographic images, provides digitized mammograms with annotations, serving as a valuable resource for diverse breast cancer research [20].

B. Methodology

The proposed methodology illustrated in Fig. 2 aims in developing a Computer-Aided Diagnosis (CAD) system for classifying mammographic images into mass, microcalcification, and normal cases. The process starts by combining datasets, then undergoes preprocessing which includes format conversion, denoising, and contrast enhancement. Subsequently, patch extraction and data augmentation methods are employed, succeeded by transfer learning.

The approach concentrates on regions of interest, thereby enhancing system's ability to detect subtle features that may indicate potential abnormalities. To further improve the robustness and generalization of the CAD system, a variety of augmentation techniques are applied to the extracted patches. Additionally, a Deep Learning (DL) architecture is integrated, leveraging its capacity to automatically learn hierarchical representations from the extracted patches, further enhancing the system's ability to classify mammographic images. Furthermore, a comparative performance analysis will be conducted against various models, allowing for an in-depth understanding of the proposed system's efficacy in comparison to existing approaches

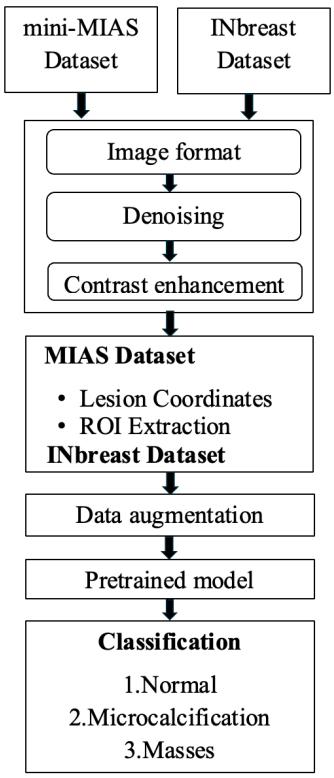

Fig. 2. Proposed methodology

C. Preprocessing

The mammogram image preprocessing pipeline involves several essential steps. Image format conversion is performed to standardize the format to PNG, ensuring compatibility and ease of access. Denoising techniques, including median filtering, are applied to reduce unwanted artifacts while preserving essential details. Additionally, a comprehensive evaluation of denoising techniques reveals that median filtering consistently outperforms mean and gaussian filtering by considering Mean Square Error (MSE), Peak Signal to noise ratio (PSNR), and Structural index similarity (SSIM) across various categories of mammographic images. This comparative analysis underscores the efficacy of median filtering in preserving image details while effectively reducing noise, thus further enhancing the overall quality and reliability of mammogram images for diagnosis and treatment planning in breast cancer diagnostics. Finally, contrast enhancement using Contrast Limited Adaptive Histogram Equalization (CLAHE) improves visual quality and diagnostic interpretability by enhancing contrast adaptively while mitigating noise amplification. Preprocessing steps collectively enhance image quality and facilitate more reliable analysis for breast cancer diagnosis.

D. Patch Extraction

In mammographic image analysis, patch extraction is essential for isolating regions of interest. The approach varies depending on whether it is lesion-focused or uses the entire image. For mini-MIAS images with lesions, extraction centers around lesion coordinates, capturing local features, where INbreast uses the entire image. Normal images are centered around the geometric center to encompass significant breast tissues. This dual approach combines local and global features, aiding in accurate diagnosis.

E. Data Augmentation

Data augmentation addresses limitations in mammographic dataset size by applying transformations that includes width and height shifts, shear, zooming, and horizontal flipping to generate additional training samples. This diversifies the dataset, enhancing the resilience of DL model by subjecting it to a broader range of conditions. It helps prevent overfitting, improving the model's ability to generalize to unseen data. By simulating real-world variations encountered in clinical practice, including changes in breast positioning, the model becomes more adaptable, ultimately enhancing diagnostic performance.

F. Resizing

Resizing images to a standard size improves computational efficiency, model compatibility, and training stability by reducing variability in input dimensions. It optimizes memory usage, enhances model generalization, ensures compatibility with pretrained models, and preserves clinical information through bilinear interpolation, essential for accurate medical imaging diagnosis.

G. Transfer Learning

In this work, enhanced efficiency and performance were achieved by employing pre-trained deep learning models including ResNet, Inception, and VGG [21]. The pretrained architecture, as shown in Fig. 3, trained on diverse datasets, offers powerful feature extraction capabilities, capturing intricate patterns. Through transfer learning, the proposed model adapts learned features to classify mammograms into mass, microcalcification, and normal categories, reducing training time and computational resources significantly. Notably, the model training process takes approximately 35-45 minutes.

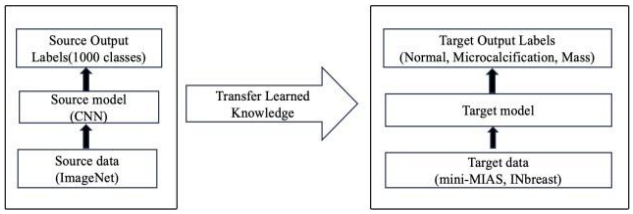

Fig. 3. Transfer learning architecture

IV. Results and Discussion

This section provides a comprehensive discussion on the outcomes of our breast cancer detection methodology which covers the performance evaluation of denoising filters, the effectiveness of contrast enhancement techniques, and details on patch extraction and data augmentation methods. Additionally, the performance of pretrained models is analyzed emphasizing the accuracy of Inception ResNet V2.

A. Performance measure of denoising filters

In the context of denoising, performance measures quantify how effectively a denoising filter reduces noise while preserving important image features, using different metrics that includes MSE, PSNR, SSIM. MSE, measures the average squared difference between corresponding pixel

intensities in the original and denoised images, with lower values indicating superior denoising performance. For an image of dimension $M \times N$, where $I(i,j)$, intensity of the original pixel and $K(i,j)$, intensity of the denoised pixel:

$$\text{MSE} = \frac{1}{MN}\sum_{i=1}^{M}\sum_{j=1}^{N}[I(i,j) - K(i,j)]^2 \quad (1)$$

Peak Signal-to-Noise Ratio (PSNR) measures the relationship between the highest potential pixel intensity and the square root of MSE. Higher PSNR values signify better image quality. The PSNR is calculated as follows:

$$\text{PSNR} = 10\, log_{10}\frac{MAX^2}{MSE} \quad (2)$$

Structural Similarity Index (SSIM) evaluates the structural resemblance by considering contrast, luminance, and structure. SSIM values range from -1 to 1, where 1 represents complete similarity. The SSIM between two images, X and Y, is computed as follows:

$$\text{SSIM(X,Y)} = \frac{(2\mu_X\mu_Y + C_1)(2\sigma_{XY} + C_2)}{(\mu_X^2 + \mu_Y^2 + C_1)(\sigma_X^2 + \sigma_Y^2 + C_2)} \quad (3)$$

where μ_X, μ_Y are the means of X and Y, σ_X, σ_Y are the standard deviations, σ_{XY} is the covariance, and C_1 and C_2 are constants to prevent division by zero.In evaluating the performance of denoising filters on both the INbreast and mini- MIAS datasets, the median filter stands out as the preferred technique based on the average MSE, PSNR, and SSIM metrics as shown in the TABLE I.

TABLE I. PERFORMANCE COMPARISON

Median Filter				
Dataset	***Category***	***Average MSE***	***Average PSNR (dB)***	***Average SSIM***
INbreast	Normal	**2.6172**	**44.6194**	**0.9687**
INbreast	Mass	**1.9709**	**46.1840**	**0.9753**
INbreast	Microcalcification	**1.9646**	**46.0278**	**0.9759**
mini-MIAS	Normal	**0.8213**	**49.2958**	**0.9887**
mini-MIAS	Mass	**0.9206**	**48.8276**	**0.9873**
mini-MIAS	Microcalcification	**0.8550**	**49.6034**	**0.9897**
Mean Filter				
Dataset	***Category***	***Average MSE***	***Average PSNR (dB)***	***Average SSIM***
INbreast	Normal	2.6688	44.3993	0.9685
INbreast	Mass	2.0382	45.8240	0.9750
INbreast	Microcalcification	2.0255	45.7366	0.9749
mini-MIAS	Normal	1.4273	46.7872	0.9862
mini-MIAS	Mass	1.5472	46.4873	0.9847
mini-MIAS	Microcalcification	1.2517	47.2416	0.9874
Gaussian Filter				
Dataset	***Category***	***Average MSE***	***Average PSNR (dB)***	***Average SSIM***
INbreast	Normal	1.9064	45.8774	0.9687
INbreast	Mass	1.4556	47.2834	0.9731
INbreast	Microcalcification	1.4467	47.1996	0.9817
mini-MIAS	Normal	1.1255	47.7886	0.9887
mini-MIAS	Mass	1.2207	47.4901	0.9873
mini-MIAS	Microcalcification	0.9926	48.2523	0.9911

The median filter consistently outperforms mean and Gaussian filters for denoising mammographic images across all categories in both INbreast and mini-MIAS datasets. It achieves high PSNR values ranging from 44.62 to 49.60 dB and SSIM values ranging from 0.97 to 0.99 preserving image quality and details effectively. Its average MSE values are notably lower having 2.62, 1.97, and 1.96 for INbreast; 0.82, 0.92, and 0.86 for mini-MIAS. This highlights the robustness and effectiveness of the median filter, making it the preferred choice for denoising.

B. Contrast Enhancement

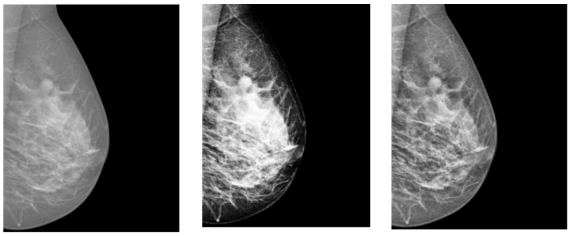

(a) (b) (c)

Fig. 4. (a) Original image (b) Histogram equalized image (c) CLAHE

While both Contrast Limited Adaptive Histogram Equalization and Histogram equalization aim to enhance contrast, the local adaptability and noise reduction capabilities of CLAHE make it the preferred choice for the mammographic image analysis. The visual improvements shown in Fig. 4, observed with CLAHE contribute to improved image quality and, consequently, enhance the effectiveness of the deep learning model in detecting and classifying abnormalities.

C. Patch Extraction

For mammographic images in the mini-MIAS dataset with annotated lesions, the extraction is centred around the identified lesion. The coordinates (x, y) and the lesion radius are utilized to define a circular region of interest. This region is then used to extract patches, ensuring that relevant local features around the lesion are captured. For normal images , as shown in Fig. 5, the extraction process is centred around a defined point, typically the geometric center of the image to encompass a substantial region, containing most of the breast tissues.

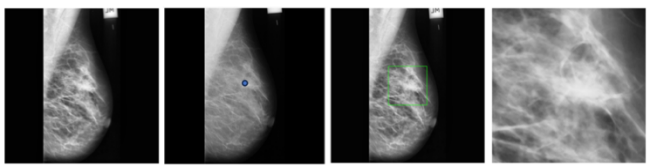

(a) (b) (c) (d)

Fig. 5. (a) Original image (b) Center location identification (c) Bounding box and coordinates (d) Extracted patch

D. Data Augmentation

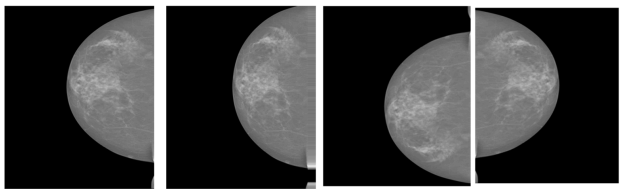

(a) (b) (c) (d)

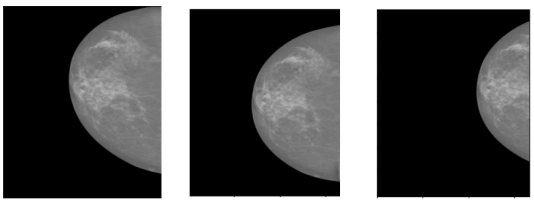

(e) (f) (g)

Fig. 6. (a) Original image (b) Zoomed image (c) Vertical flipped image (d) Horizontal flipped image (e) Sheared image (f) Height shift (g) Width shift

Images shown in Fig. 6, subjected to traditional augmentation techniques including zoom, shear, width shift, height shift, horizontal and vertical flip to diversify the dataset and enhance model robustness. These transformations introduce variations in the images while preserving their semantic content, resulting in a larger and more diverse dataset for improved model performance and generalization.

E. Performance of Pretrained model

TABLE II. TEST LOSS AND ACCURACY OF EACH MODEL

Model	Test Loss	Test Accuracy
ResNet-50	1.0928	0.8905
ResNet-101	0.7123	0.9733
ResNet-152	1.1670	0.8076
Inception V3	0.2323	0.9646
Inception ResNet V2	**0.2484**	**0.9793**
VGG-16	0.2558	0.8964
VGG-19	0.3538	0.8639

The proposed work is evaluated with various pretrained models on the test dataset as shown in TABLE II, with Inception ResNet V2 showing exceptional performance, achieving a test loss of 0.2484 and a test accuracy of 0.9793. This outperformed other models which includes ResNet and VGG, indicating the effectiveness of Inception ResNet V2's architectural enhancements in capturing intricate features. These findings emphasize the importance of model selection for optimal performance in image classification tasks, highlighting Inception ResNet V2 as a strong model with high accuracy and lower loss. Each model has undergone hyperparameter tuning that aids to mitigate overfitting, thereby enhancing the generalization capability of the models.

TABLE III. HYPERPARAMETER TUNING OF INCEPTION RESNET V2 PRE-TRAINED MODEL

Learning rate		Epochs		Regularization	Accuracy
Frozen layers	*Fine tuning*	*Frozen layers*	*Fine tuning*		
0.01	0.001	30	50	-	0.8613
0.01	0.0001	30	50	-	0.8672
0.01	0.0021	30	50	-	0.9085
0.01	0.0011	30	50	-	0.9380
0.01	0.0005	30	50	-	0.9439
0.001	0.0001	30	50	-	0.9646
0.001	**0.0001**	**30**	**50**	**L2(0.01)**	**0.9793**

From the TABLE III results of hyperparameter tuning of the Inception ResNet V2, identified optimal settings for learning rates, epochs, and regularization during frozen layer training and fine-tuning. The suitable configuration, with a learning rate of 0.001 in frozen layers and 0.0001 in fine-tuning, along with L2 regularization (0.01), achieved an accuracy of 0.9793. These findings highlight the critical role of hyperparameter selection in maximizing the ability of complex DL models, specifically in transfer learning.

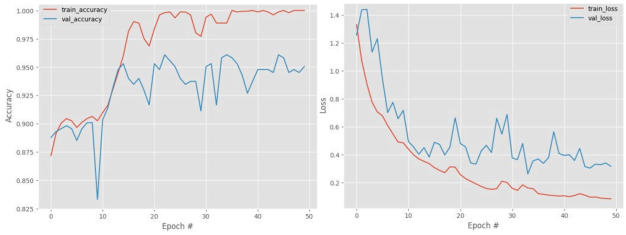

(a) (b)

Fig. 7. (a) Training and validation loss of Inception ResNet V2 (b) Training and Validation accuracy of Inception ResNet V2

Training and validation loss are crucial metrics in evaluating a model's performance. Training loss (depicted in red) as shown in Fig. 7 (a) measures the error during training, gradually decreasing as the model learns from data. Validation loss (in blue) as shown in Fig. 7 (b) assesses the model's generalization to new data. Concurrently decreasing training and validation losses indicate effective learning and generalization. Monitoring both prevents overfitting, ensuring the model does not memorize but learns to predict accurately. Similarly, training and validation accuracy measure performance, with a rising red line signifying improved training data understanding. Balancing accuracy and loss ensure a robust, well-generalizing machine learning model.

TABLE IV. CLASSIFICATION REPORT OF DIFFERENT MODELS

		Precision	Recall	F1-Score
ResNet-50	Microcalcification	1.00	0.98	0.99
	Mass	0.87	0.77	0.82
	Normal	0.93	0.98	0.95
ResNet-101	Microcalcification	0.99	0.99	0.99
	Mass	0.94	0.83	0.88
	Normal	0.95	0.99	0.97
ResNet-152	Microcalcification	0.99	0.98	0.99
	Mass	0.88	0.60	0.71
	Normal	0.88	0.98	0.93
Inception V3	Microcalcification	0.99	0.99	0.99
	Mass	0.93	0.74	0.83
	Normal	0.94	0.99	0.96
Inception ResNet V2	**Microcalcification**	**0.99**	**0.99**	**0.99**
	Mass	**0.97**	**0.83**	**0.89**
	Normal	**0.97**	**1.00**	**0.98**
VGG-16	Microcalcification	1.00	0.96	0.98
	Mass	0.71	0.57	0.63
	Normal	0.86	0.97	0.92
VGG-19	Microcalcification	0.98	0.97	0.98
	Mass	0.62	0.14	0.23
	Normal	0.79	0.97	0.87

From the classification report as shown in TABLE IV, the Inception ResNet V2 model demonstrates excellent performance across multiple metrics. It achieves high precision, recall, and F1-score for calcification: 0.99 precision, mass: 0.97 precision, 0.83 recall, 0.89 F1-score, and normal: 0.97 precision, 1.00 recall, 0.98 F1-score. With an overall accuracy of 98%, the model effectively predicts across all classes, showcasing strength in distinguishing between calcification, mass, and normal instances,

highlighting its proficiency in classifying mammographic images.

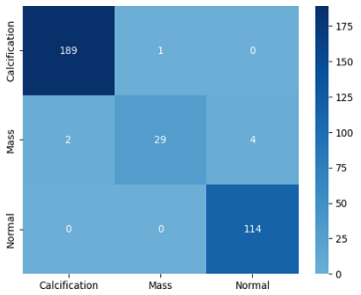

Fig. 8. Confusion matrix of Inception Resnet V2

The confusion matrix for the Inception ResNet V2 model reveals best accuracy in classifying calcification as shown in Fig. 8, with only 1 incorrect prediction out of 190 instances. For Mass, the model achieved 29 true positives but had 2 false positives and missed 4 instances (false negatives).

TABLE V. COMPARISON BETWEEN PROPOSED AND EXISTING METHODS

Reference	Database	Accuracy	F1-Score	Sensitivity	Specificity
Kermouni et al. [6]	INbreast	-	-	0.9866	0.9777
X.Yu et al. [10]	MIAS and INbreast	95.74%	-	0.9283	0.9855
A. Baccouche et al. [12]	Private dataset	92.09	-	-	-
F. Mohanty et al. [14]	MIAS and DDSM	100%	-	-	-
Proposed approach	MIAS and INbreast	97.93%	0.9557	0.9411	0.9885

The proposed methodology achieves an accuracy of 97.93% in mammographic image analysis, focusing on identifying normal cases alongside microcalcifications and masses. With 0.9411 sensitivity and 0.9885 specificity the method ensures a reliable detection of both positive and negative instances as depicted in TABLE V. Despite broader focus on breast abnormalities from the state-of-the-art methodologies, the proposed methodology maintains competitive performance by targeting critical indicators of breast pathology and provides valuable insights into mammographic analysis excelling in specific abnormality detection while maintaining robust performance across datasets and classes.

V. CONCLUSION AND FUTURE SCOPE

The proposed work enhances breast cancer diagnosis through effective analysis of mammographic images. Pre-processing enhances the image quality for subsequent analyses, while patch extraction diversifies the dataset, improving deep-learning model robustness. Various pre-trained models include ResNet-50,101,152 layers, VGG-16,19 layers, Inception V3 and Inception ResNet V2 were modeled and analyzed. The proposed approach with Inception ResNet V2 achieves an accuracy of 97.93%, sensitivity of 0.9411, and specificity of 0.9885, highlighting the significance of the choice of model. Future efforts will focus on distinguishing between benign and potentially malignant abnormalities, enhancing diagnostic precision. This approach aims to provide healthcare professionals with clearer insights, aiding in informed patient care decisions and advancing breast cancer diagnostics.

REFERENCES

[1] Report from Global Cancer Observatory [Online], Available: https://gco.iarc.fr/. [Accessed: 25-Jan-2023].

[2] M. Akram, M. Iqbal, M. Daniyal, and A. U. Khan, "Awareness and current knowledge of breast cancer," *Biol Res*, Dec. 2017, vol. 50, no. 1, pp. 33.

[3] S. V. J. Jaikrishnan, O. Chantarakasemchit and P. Meesad, "A Breakup Machine Learning Approach for Breast Cancer Prediction," *ICITEE*, Thailand, Oct. 2019, pp. 1–6.

[4] Srinivashini. N and Lavanya. R, "False Positive Reduction in Mammographic Mass Detection Using Image Representations for Textural Analysis," *CCCSP*, Chennai, India, 2021, pp. 1-6.

[5] S. Shrinithi, D. Vijayan, and R. Lavanya, "Computer aided diagnosis system for breast density classification in mammograms," *J. Phys.: Conf. Ser.*, Aug. 2022, vol. 2318, no. 1, pp. 012039.

[6] Vijayan, Devi, and R. Lavanya, "Ensemble of density-specific experts for mass characterization in mammograms," *Signal Image Video Process*., Jan. 2021, vol. 15, no. 5, pp. 1011-1019.

[7] S.Li, M.Dong, G.Du and X.Mu, "Attention Dense-U-Net for Automatic Breast Mass Segmentation in Digital Mammogram," *IEEE Access*, 2019, vol. 7, pp. 59037–59047.

[8] Logullo AF, Prigenzi KCK, Nimir CCBA and Franco AFV, "Breast microcalcifications: Past, present and future (Review)," *Mol Clin Oncol*, Feb. 2022, vol. 16, no. 4, pp. 81.

[9] Nisha. K.L, Sreelekha. G, Sathidevi. P.S, Mohanachandran. P and Vinekar. A, "A computer-aided diagnosis system for plus disease in retinopathy of prematurity with structure adaptive segmentation and vessel based features," *Comput Med Imaging Graph*., 2019, vol. 74, pp. 72-94.

[10] N. Kermouni Serradj, M. Messadi, and S. Lazzouni, "Classification of Mammographic ROI for Microcalcification Detection Using Multifractal Approach," *J Digit Imaging*, Dec. 2022, vol. 35, pp. 1544–1559.

[11] H. Cao, S. Pu, W. Tan, J. Tong, and D. Zhang, "Multi- Tasking U-Shaped Network for Benign and Malignant Classification of Breast Masses," *IEEE Access*, 2020, vol. 8, pp. 223396–223404.

[12] E. M. F. El Houby and N. I. R. Yassin, "Malignant and non-malignant classification of breast lesions in mammograms using convolutional neural networks," *Biomed. Signal Process. Control.*, Sep. 2021, vol.70, pp. 102954.

[13] X. Yu, C. Kang, D. S. Guttery, S. Kadry, Y. Chen, and Y.D. Zhang, "ResNet-SCDA-50 for Breast Abnormality Classification," *IEEE/ACM Trans. Comput. Biol. Bioinform*, Jan. 2021, vol. 18, no. 1, pp. 94-102.

[14] N. A. N. Azlan, C.-K. Lu, I. Elamvazuthi and T. B. Tang, "Automatic Detection of Masses, From Mammographic Images via Artificial Intelligence Techniques," *IEEE Sens. J.*, Nov. 2020, vol. 20, no. 21, pp. 13094–13102.

[15] R. Rabidas and W. Arif, "Characterization of mammographic masses based on local photometric attributes," *Multim. Tools Appl*, Aug. 2020, vol. 79, no. 29–30, pp. 21967–21985.

[16] A. Baccouche, B. Garcia-Zapirain, Y. Zheng, and A. S. Elmaghraby, "Early detection and classification of abnormality in prior mammograms using image-to-image translation and YOLO techniques," *Comput. Methods Programs Biomed*, Jun. 2022, vol. 221, pp. 106884.

[17] X. Shu, L. Zhang, Z. Wang, Q. Lv and Z. Yi, "Deep Neural Networks With Region-Based Pooling Structures for Mammographic Image Classification," *IEEE Trans. Med. Imaging*, Jun. 2020, vol. 39, no. 6, pp. 2246–2255.

[18] F. Mohanty, S. Rup, B. Dash, B. Majhi and M. N. S. Swamy, "Digital mammogram classification using 2D-BDWT and GLCM features with FOA-based feature selection approach," *Neural Comput. Appl*., Jun. 2020, vol. 32, no. 11, pp. 7029–7043.

[19] The INbreast Dataset [Online], Available: http://medicalresearch.inescporto.pt/breastresearch/index.php/Get_INbreast_Database. [Accessed: 02-Jan-2023].

[20] The mini-MIAS database of mammograms [Online], Available: http://peipa.essex.ac.uk/info/mias.html. [Accessed: 02-Jan-2023].

[21] G. Suguna and R. Lavanya, "Performance Assessment of EyeNet Model in Glaucoma Diagnosis," *Pattern Recognit. Image Anal*., Apr. 2021, vol. 31, no. 2, pp. 334-344.